Supplementary information files for Empowering catalyst supports: A new concept for catalyst design demonstrated in the Fischer–Tropsch synthesis

Empowering catalyst supports – A new concept for catalyst design demonstrated in the Fischer-Tropsch synthesis

Motlokoa Khasu,[a] Wijnand Marquart,[a] Patricia J. Kooyman,[a] Charalampos Drivas,[b,c] Mark A. Isaacs,[b,d] Alexander J. Mayer,[e] Sandie E. Dann,[e] Simon A. Kondrat,[e] Michael Claeys,[a] and Nico Fischer[*a]*

[a] DSI-NRF Centre of Excellence in Catalysis c*change and Catalysis Institute, Department of Chemical Engineering, University of Cape Town, 7701, Rondebosch, Cape Town, South Africa

[b] HarwellXPS, Research Complex at Harwell, Rutherford Appleton Lab, Didcot OX11 0FA, United Kingdom

[c] Department of Chemical Engineering and Analytical Science, University of Manchester, Manchester M13 9PL, UK.

[d] Department of Chemistry, University College London, 20 Gower Street, London, WC1H 0AJ, United Kingdom

[e] Department of Chemistry, Loughborough University, Loughborough, LE11 3TU, United Kingdom

* Corresponding author: nico.fischer@uct.ac.za

Table S1. Elemental composition of synthesised perovskite materials, apparent experimental composition based on the elemental composition, and γ-Fe_2O_3 loading on catalyst precursors. Numbers in brackets indicate the targeted composition assuming $\delta = 0$. Some samples have been prepared in multiple batches to cater for the different characterization and testing protocols.

	Composition of perovskite materials					Iron oxide loading
	La (wt.-%)	K (wt.-%)	Al (wt.-%)	Mn (wt.-%)	apparent experimental composition	γ-Fe_2O_3 (wt.-%)
$LaAlO_{3-\delta}$	67.9 (64.9)	0.0 (0.0)	12.1 (12.6)	0.0 (0.0)	$La_{1.04}Al_{0.96}O_{3-\delta}$	17.3 (20.0)
$La_{0.9}K_{0.1}AlO_{3-\delta}$ [a]	61.8 (61.3)	2.1 (1.9)	11.9 (13.2)	0.0 (0.0)	$La_{0.95}K_{0.11}Al_{0.94}O_{3-\delta}$	n/a
$La_{0.9}K_{0.1}AlO_{3-\delta}$ [b]	68.1 (61.3)	1.8 (1.9)	12.8 (13.2)	0.0 (0.0)	$La_{0.97}K_{0.09}Al_{0.97}O_{3-\delta}$	18.7 (20.0)
$La_{0.9}K_{0.1}AlO_{3-\delta}$ [c]	64.8 (61.3)	1.5 (1.9)	12.9 (13.2)	0.0 (0.0)	$La_{0.95}K_{0.08}Al_{0.97}O_{3-\delta}$	19.2 (20.0)
$LaAl_{0.8}Mn_{0.2}O_{3-\delta}$	62.2 (63.3)	0.0 (0.0)	9.7 (9.8)	3.2 (5.0)	$La_{1.03}Al_{0.83}Mn_{0.13}O_{3-\delta}$	17.3 (20.0)
$La_{0.9}K_{0.1}Al_{0.8}Mn_{0.2}O_{3-\delta}$	63.6 (59.7)	1.2 (1.9)	10.9 (10.3)	4.1 (5.2)	$La_{0.95}K_{0.06}Al_{0.84}Mn_{0.15}O_{3-\delta}$	19.4 (20.0)
$LaAl_{0.4}Mn_{0.6}O_{3-\delta}$	63.2 (60.2)	0.0 (0.0)	4.2 (4.7)	10.2 (14.3)	$La_{1.14}Al_{0.39}Mn_{0.47}O_{3-\delta}$	19.0 (20.0)
$La_{0.9}K_{0.1}Al_{0.4}Mn_{0.6}O_{3-\delta}$ [a]	66.8 (56.7)	1.2 (1.8)	5.3 (4.9)	10.4 (14.9)	$La_{1.07}K_{0.07}Al_{0.44}Mn_{0.42}O_{3-\delta}$	n/a
$La_{0.9}K_{0.1}Al_{0.4}Mn_{0.6}O_{3-\delta}$ [b]	60.4 (56.7)	0.9 (1.8)	5.9 (4.9)	11.5 (14.9)	$La_{0.98}K_{0.05}Al_{0.49}Mn_{0.47}O_{3-\delta}$	19.2 (20.0)
$LaMnO_{3-\delta}$	57.6 (57.4)	0.0 (0.0)	0.0 (0.0)	15.1 (22.7)	$La_{1.20}Mn_{0.80}O_{3-\delta}$	17.2 (20.0)
$La_{0.9}K_{0.1}MnO_{3-\delta}$	63.0 (53.9)	1.2 (1.7)	0.0 (0.0)	16.0 (23.7)	$La_{1.17}K_{0.08}Mn_{0.75}O_{3-\delta}$	20.0 (20.0)

[a] Sample specifically prepared for XANES analysis.

[b] Sample used for FT performance at a space velocity of 8 $mL \cdot min\text{-}1 \cdot g_{catalyst}^{-1}$.

[c] Sample used for FT performance at an elevated space velocity of 30 $mL \cdot min\text{-}1 \cdot g_{catalyst}^{-1}$.

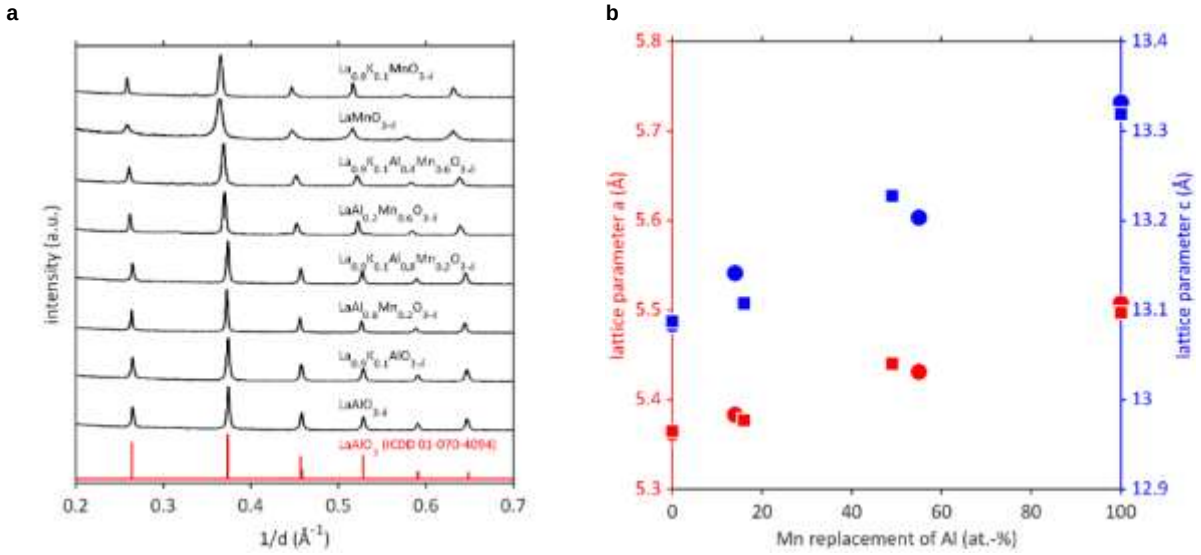

Figure S1. XRD characterisation of synthesized $La_{1-x}K_xAl_{1-y}Mn_yO_{3-\delta}$ perovskites. **a**, Experimental X-ray diffraction patterns of $La_{1-x}K_xAl_{1-y}Mn_yO_{3-\delta}$ with x = 0 or 0.1 and y = 0, 0.2, 0.6 or 1. Reference pattern of $LaAlO_3$ from the International Centre for Diffraction Data Powder Diffraction File 4+ 2020 (entry 01-070-1094). **b**, Lattice parameter a (red) and c (blue) of $La_{1-x}K_xAl_{1-y}Mn_yO_{3-\delta}$ with x = 0 or 0.1 and y = 0, 0.2, 0.6 or 1 as function of targeted Mn replacement of Al. Square markers represent perovskites with a targeted 10% of lanthanum atoms replaced by potassium atoms.

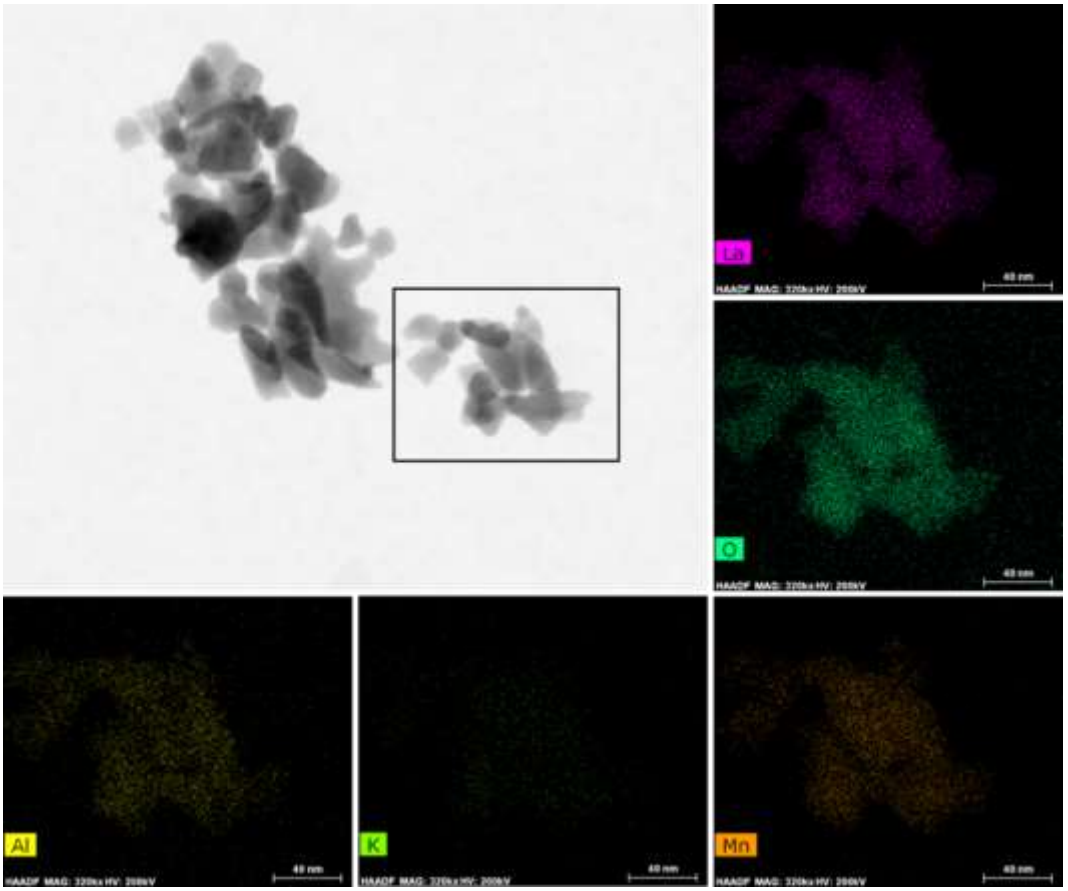

Figure S2. STEM brightfield micrograph of $La_{0.9}K_{0.1}Al_{0.4}Mn_{0.2}O_{3-\delta}$ after reductive pre-treatment, and individual EDS maps of constituting elements.

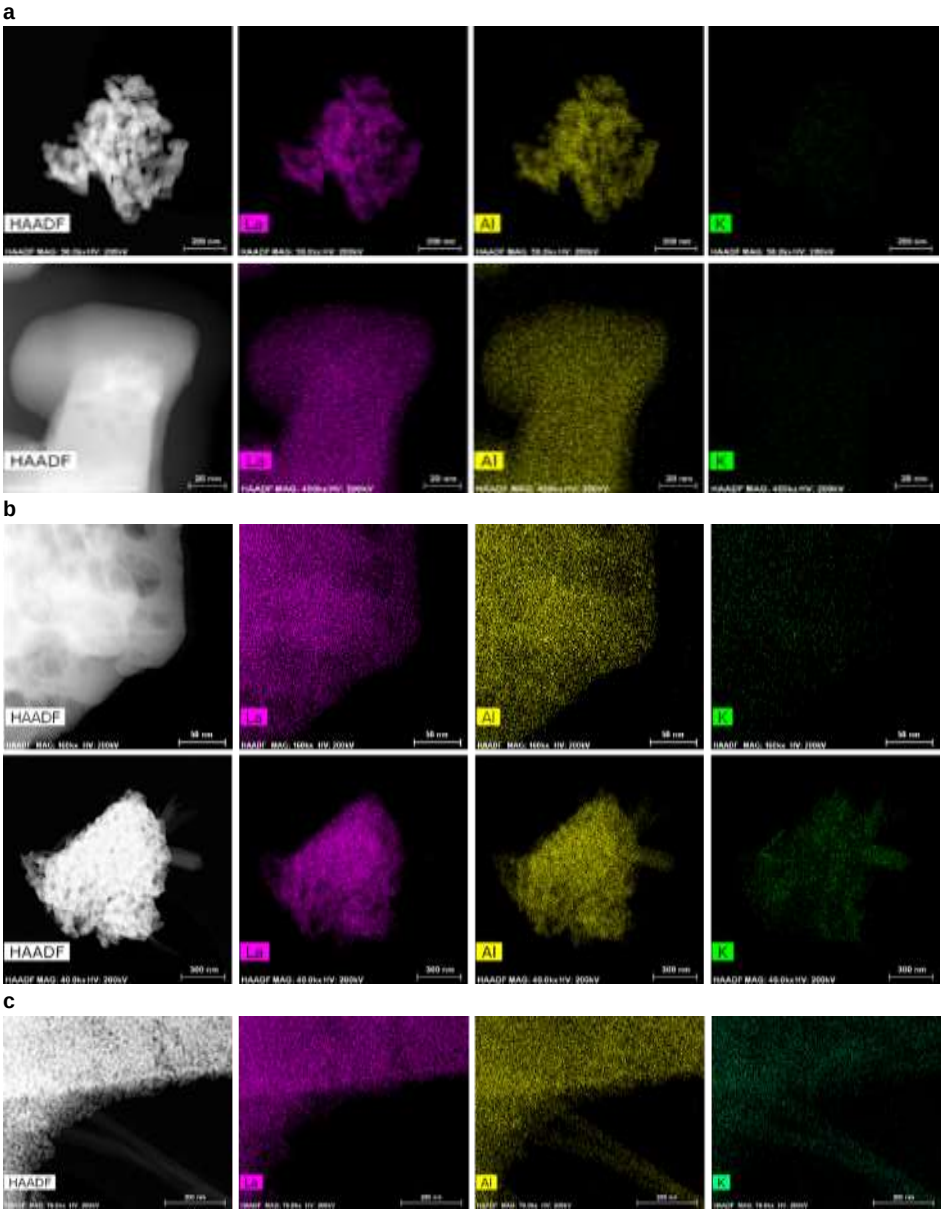

Figure S3. HAADF STEM micrograph after reductive treatment, and individual EDS maps of constituting elements. **a**, $LaAlO_{3-\delta}$ after reductive pre-treatment; **b**, K impregnated $1K/LaAlO_{3-\delta}$ after reductive pre-treatment; **c**, $La_{0.9}K_{0.1}AlO_{3-\delta}$ before reductive pre-treatment.

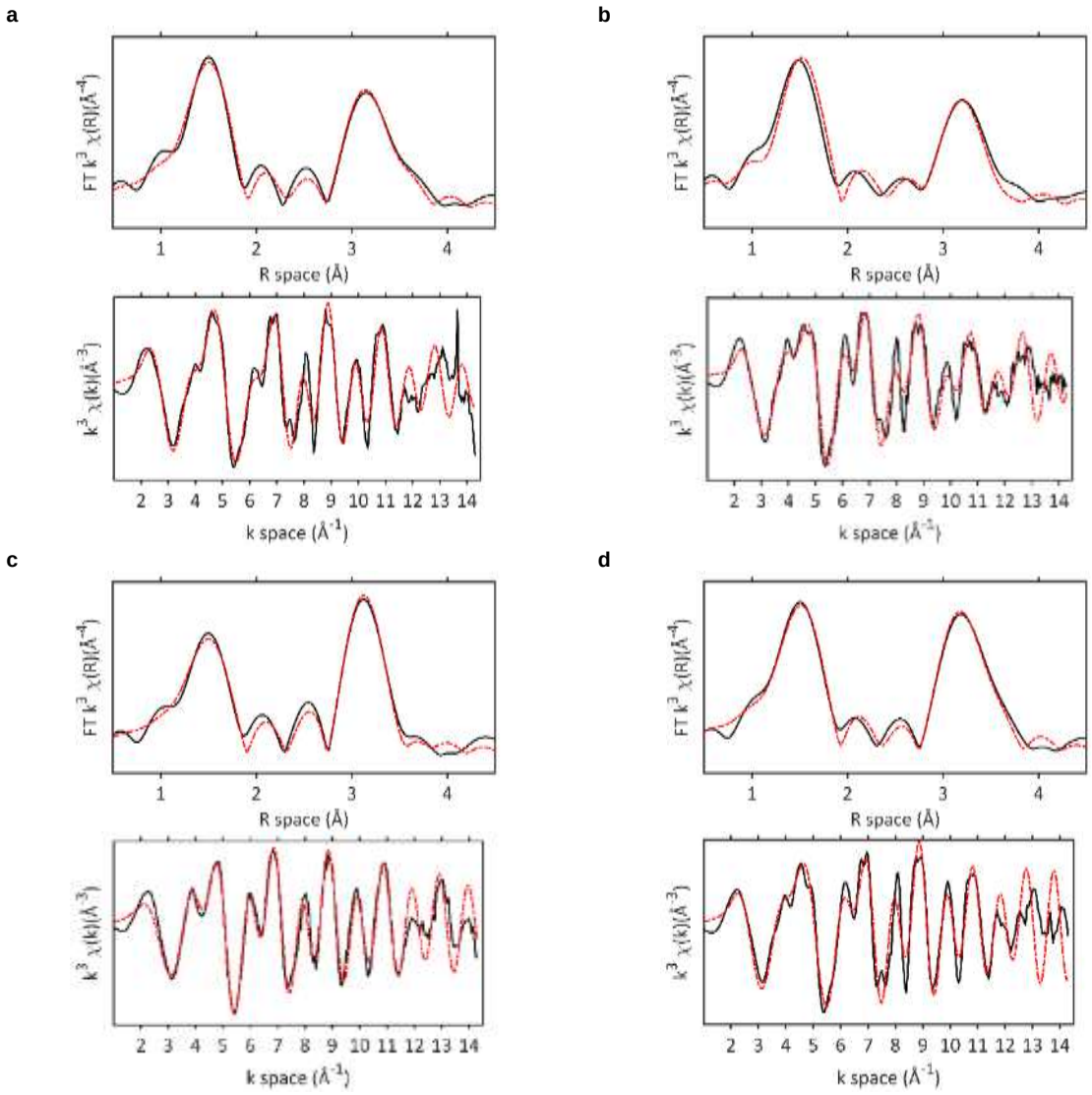

Figure S4. Manganese K-edge EXAFS fitting of $La_{0.9}K_{0.1}Al_{1-y}Mn_yO_{3-\delta}$ perovskites. Top graphs display a comparison of data (black) and fit (red) of the magnitude of the Fourier Transform of the EXAFS χ data. Bottom graphs display a comparison of data (black) and fit (red) of the k^3 weighted data. **a**, $La_{0.9}K_{0.1}MnO_{3-\delta}$; **b**, $La_{0.9}K_{0.1}MnO_{3-\delta}$ pre-reduced; **c**, $La_{0.9}K_{0.}1Al_{0.4}Mn_{0.6}O_{3-\delta}$ pre-reduced; **d**, $LaMnO_3$ standard.

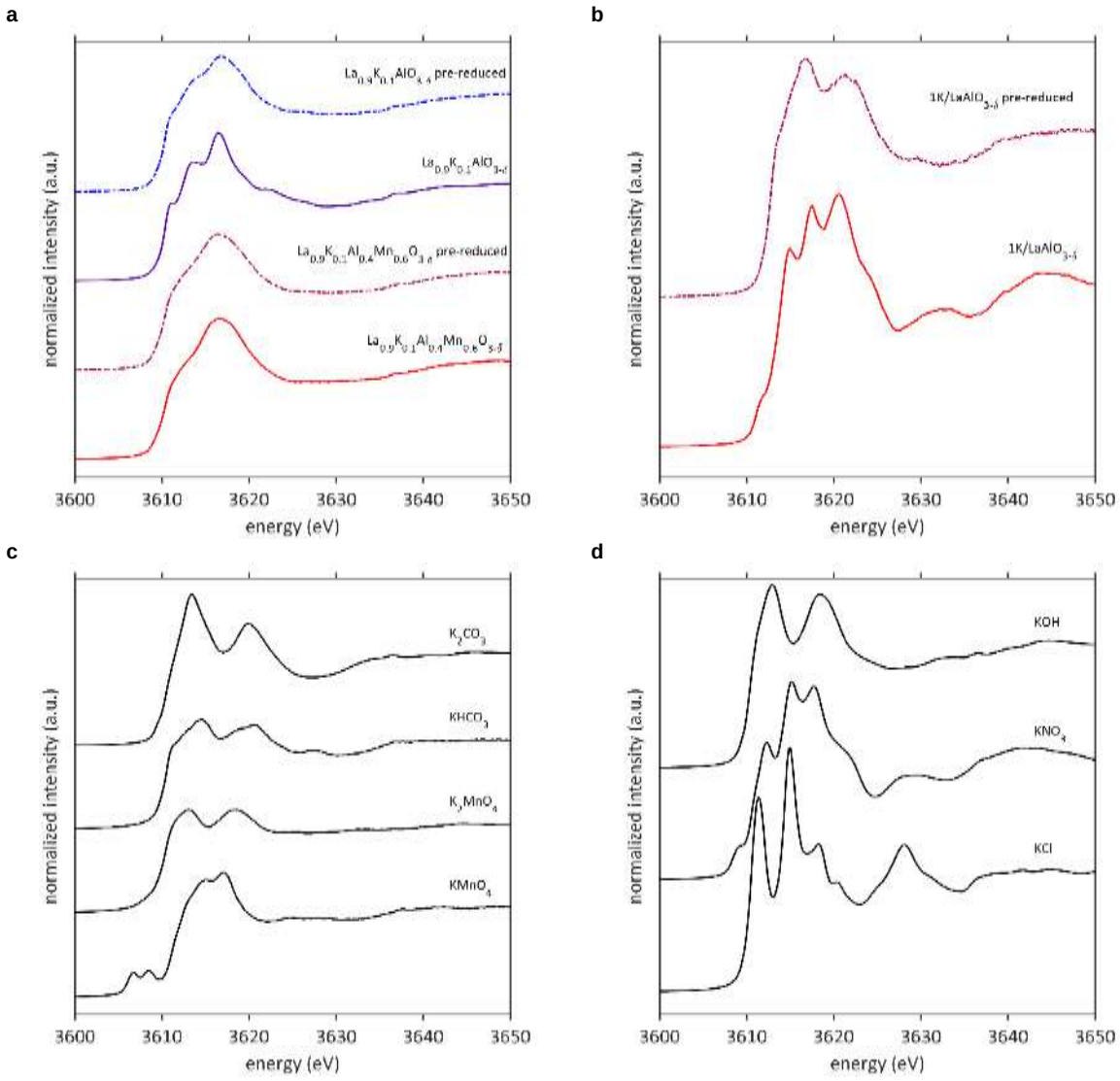

Figure S5. XANES of the potassium K-edge. **a**, $La_{0.9}K_{0.1}Al_{0.4}Mn_{0.6}O_{3-\delta}$ and $La_{0.9}K_{0.1}AlO_{3-\delta}$ as prepared and after reductive pre-treatment. **b**, $1K/LaAlO_{3-\delta}$ as prepared and after reductive pre-treatment. **c & d**, selected K standards.

Table S2. Surface elemental composition of $LaAlO_{3-\delta}$, $La_{0.9}K_{0.1}Al_{0.4}Mn_{0.6}O_{3-\delta}$ and $La_{0.9}K_{0.1}AlO_{3-\delta}$ determined by XPS.

Sample	Species composition								
	Al at.-%	C-O at.-%	C=O at.-%	CC-CH at.-%	K at.-%	La at.-%	Mn at.-%	O at.-%	Carbonates/CO_2 at.-%
$LaAlO_{3-\delta}$	13.6	3.2	1.3	13.7	0.0	18.0	0.0	47.8	2.4
$La_{0.9}K_{0.1}AlO_{3-\delta}$	15.7	3.2	1.9	10.0	6.1	8.0	0.0	50.6	4.5
$La_{0.9}K_{0.1}AlO_{3-\delta}$ pre-reduced	15.5	2.9	1.1	11.4	4.5	11.6	0.0	49.5	3.5
$La_{0.9}K_{0.1}Al_{0.8}Mn_{0.2}O_{3-\delta}$	6.8	2.6	1.2	12.1	1.9	18.0	5.9	48.8	2.8
$La_{0.9}K_{0.1}Al_{0.8}Mn_{0.2}O_{3-\delta}$ pre-reduced	5.8	2.2	1.0	12.2	2.3	15.5	5.5	51.1	4.5

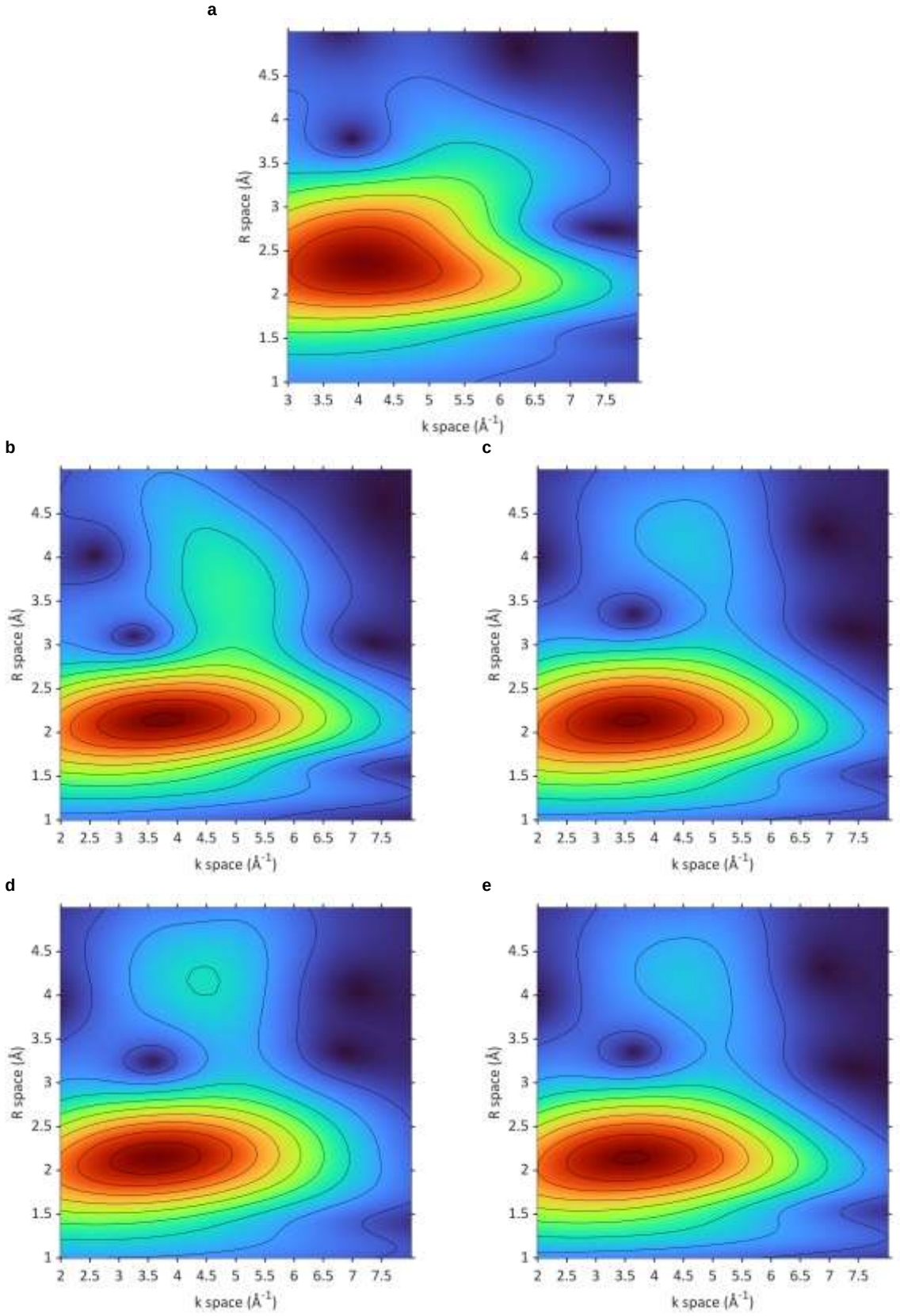

Figure S6. Wavelet transformation of k^1 data from potassium K-edge EXAFS. **a**, K_2CO_3; **b**, $La_{0.9}K_{0.1}AlO_{3-\delta}$; **c**, $La_{0.9}K_{0.1}AlO_{3-\delta}$ pre-reduced; **d**, $La_{0.9}K_{0.1}Al_{0.4}Mn_{0.6}O_{3-\delta}$; **e**, $La_{0.9}K_{0.1}Al_{0.4}Mn_{0.6}O_{3-\delta}$ pre-reduced.

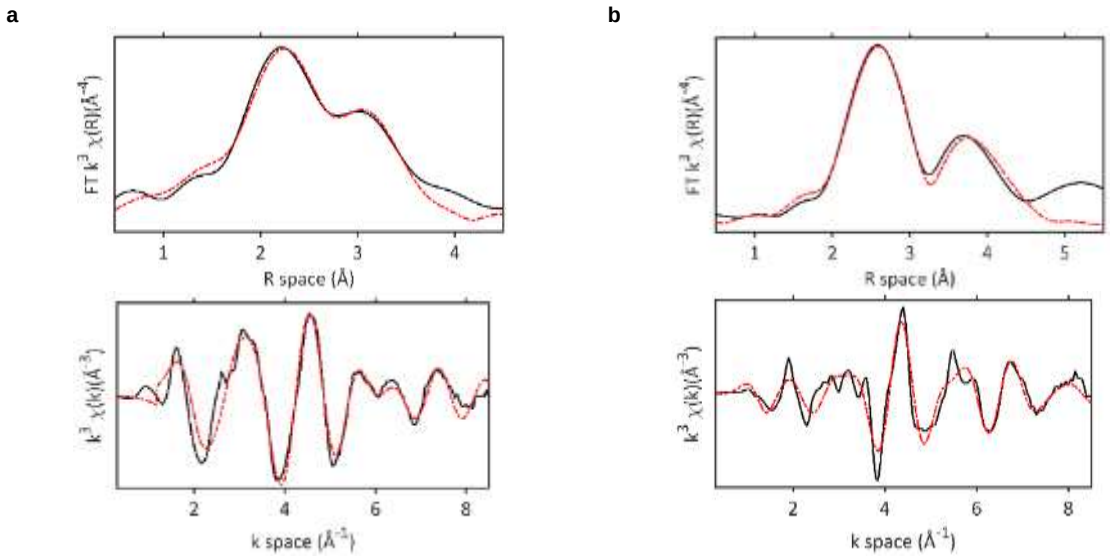

Figure S7. Potassium K-edge EXAFS fitting of K_2CO_3 and KCl standards. Top graphs display a comparison of data (black) and fit (red) of the magnitude of the Fourier Transform of the EXAFS χ data. Bottom graphs display a comparison of data (black) and fit (red) of the k^3 weighted data. **a**, K_2CO_3; **b**, KCl.

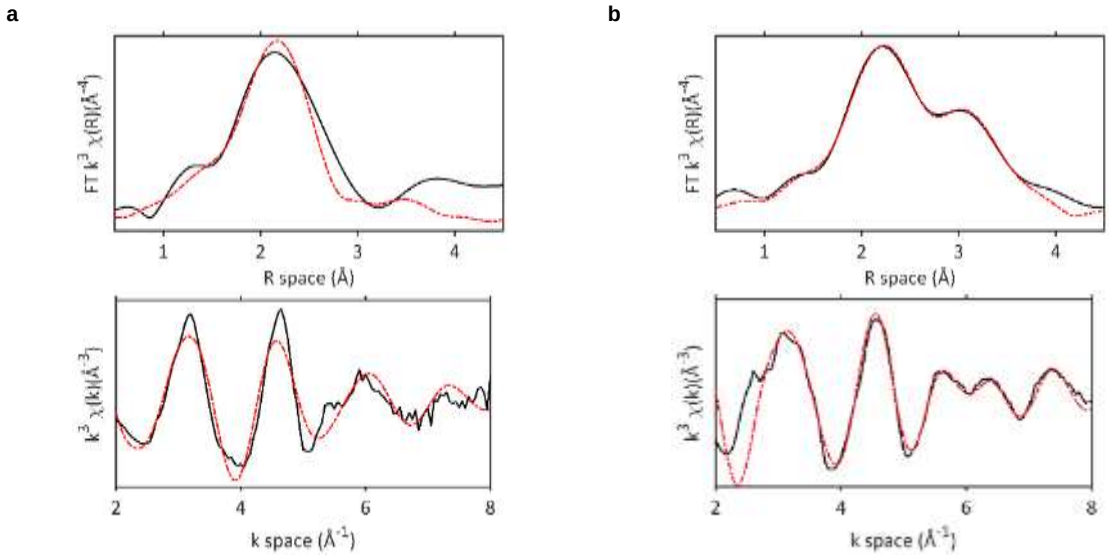

Figure S8. Fitting of the potassium K-edge EXAFS spectra of pre-reduced $La_{0.9}K_{0.1}Al_{0.4}Mn_{0.6}O_{3-\delta}$ perovskite supports with K_2CO_3 model. Top graphs display a comparison of data (black) and fit (red) of the magnitude of the Fourier Transform of the EXAFS χ data. Bottom graphs display a comparison of data (black) and fit (red) of the k^3 weighted data. **a**, $La_{0.9}K_{0.1}Al_{0.4}Mn_{0.6}O_{3-\delta}$ pre-reduced fitted with K_2CO_3 model; **b**, K_2CO_3 fitted with $La_{0.9}K_{0.1}Al_{0.4}Mn_{0.6}O_{3-\delta}$ model.

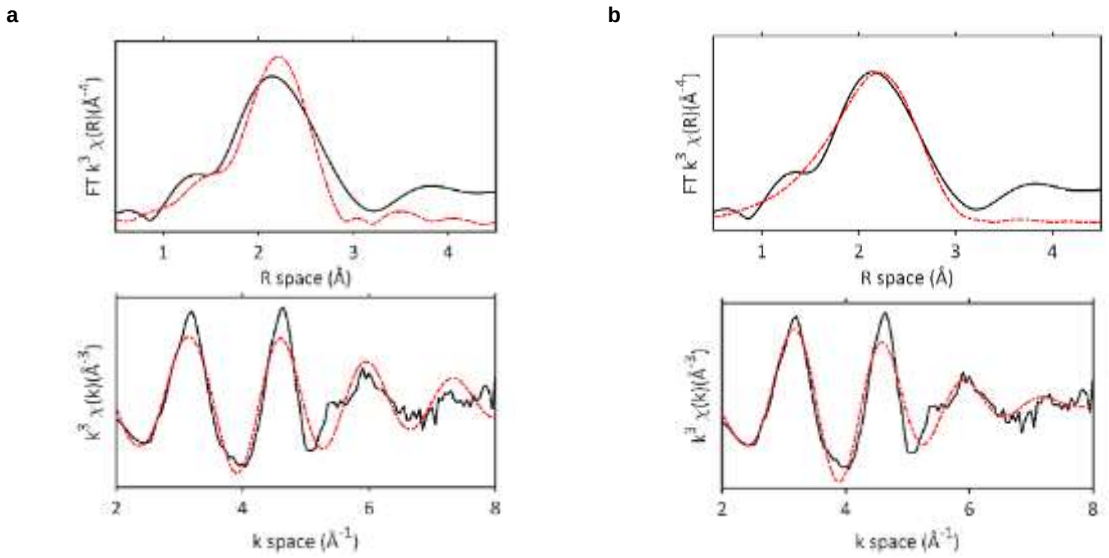

Figure S9. Fitting of the potassium K-edge EXAFS spectra of pre-reduced $La_{0.9}K_{0.1}Al_{0.4}Mn_{0.6}O_{3-\delta}$ perovskite supports with KOH or K_2O model. Top graphs display a comparison of data (black) and fit (red) of the magnitude of the Fourier Transform of the EXAFS χ data. Bottom graphs display a comparison of data (black) and fit (red) of the k^3 weighted data. **a**, $La_{0.9}K_{0.1}Al_{0.4}Mn_{0.6}O_{3-\delta}$ pre-reduced fitted with KOH model; **b**, $La_{0.9}K_{0.1}Al_{0.4}Mn_{0.6}O_{3-\delta}$ pre-reduced fitted with K_2O.

Table S3. Potassium K-edge EXAFS fitting values for pre-reduced $La_{0.9}K_{0.1}Al_{0.4}Mn_{0.6}O_{3-\delta}$ fitted with K_2CO_3, KOH, and K_2O models, and K_2CO_3 fitted using perovskite paths.

Sample	Scattering Path	Coordination Number[a]	$2\sigma^2$ (Å^2)	R (Å)	*delr*	E_f (eV)	R_{factor} *Reduced chi-square*[c]
$La_{0.9}K_{0.1}Al_{0.4}Mn_{0.6}O_{3-\delta}$ pre-reduced- (K_2CO_3 fit)	K-O K-K	7.5 2.5	0.024(3) 0.03(2)	2.76(3) 3.78(9)	-0.09(3) 0.26(9)	5(1)	0.047 (612.3)
$La_{0.9}K_{0.1}Al_{0.4}Mn_{0.6}O_{3-\delta}$ pre-reduced- (KOH fit)	K-O K-K	6 2	0.018(3) 0.05(5)	2.77(3) 3.9(2)	-0.07(3) -0.01(3)	6(1)	0.062 (677.8)
$La_{0.9}K_{0.1}Al_{0.4}Mn_{0.6}O_{3-\delta}$ pre-reduced- (K_2O fit)	K-O K-K	4 6	0.04(1) 0.035(7)	2.61(7) 2.92(5)	-0.18(7) -0.30(5)	7(2)	0.031 (305.2)
K_2CO_3	K-O 1.1 K-O 1.2 K-O 1.3 K-Mn K-La	3 5 3 8 6	0.026(34) 0.04(4) 0.02(1)	2.6(1) 3(4) 3(7) 3.7(1) 4.0(1)	0.1(1) 0(4) 0(7) 0.2(1) -0.3(1)	-0.386[b]	0.0075 (1032.4)

Fixed parameters: $S_o^2 = 1.002$ calculated from KCl standard.
[a] Coordination number fixed. [b] Fixed energy shift. [c] Value given in brackets.

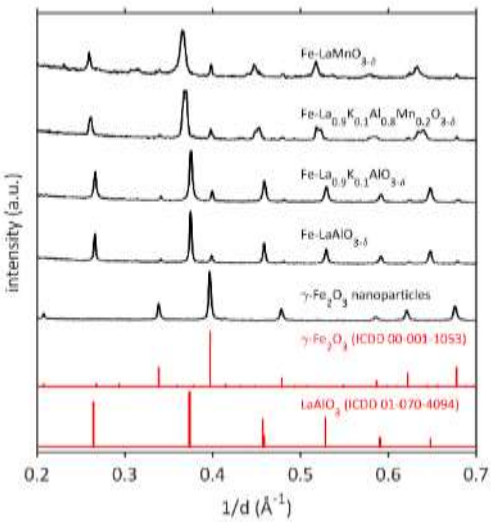

Figure S10. XRD characterisation of synthesized γ-Fe_2O_3 nanoparticles. Experimental X-ray diffraction patterns of synthesized γ-Fe_2O_3 nanoparticles as well as maghemite particles supported on selected perovskites. Reference pattern of $LaAlO_3$ and γ-Fe_2O_3 from the International Centre for Diffraction Data Powder Diffraction File 4+ 2020 (entries 01-070-1094 and 01-089-5894, respectively).

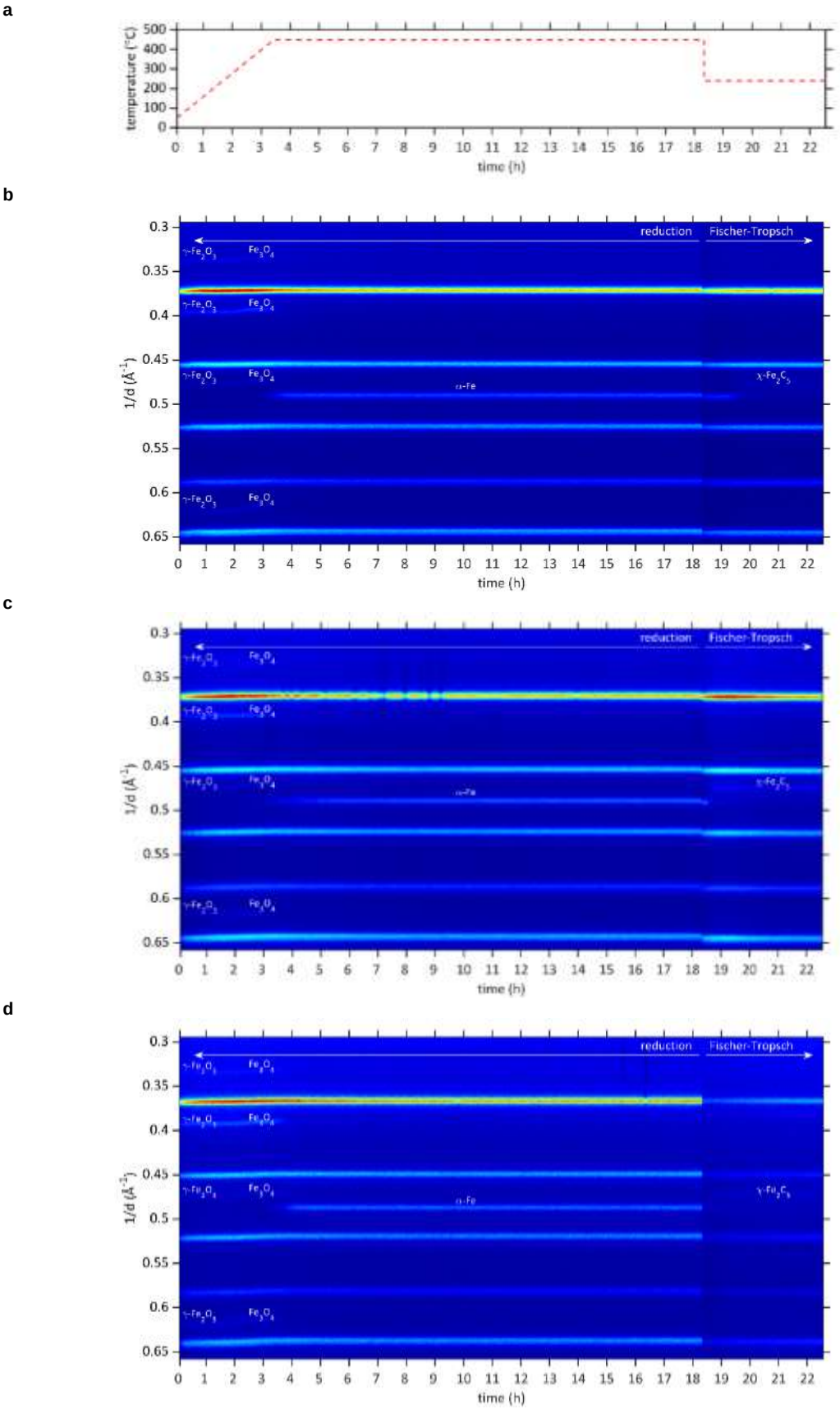

Figure S11. *In situ* XRD of synthesised catalysts during reduction and FT synthesis as function of time on stream. **a**, Sample temperature. **b**, Experimental X-ray diffraction patterns of Fe-$LaAlO_3$. **c**, Experimental X-ray diffraction patterns of Fe-$La_{0.9}K_{0.1}AlO_3$. **d**, Experimental X-ray diffraction patterns of Fe-$La_{0.9}K_{0.1}Al_{0.8}Mn_{0.2}O_{3-\delta}$.

The samples were heated in a continuous flow of H_2 at atmospheric pressure (40 $mL \cdot min^{-1} \cdot g_{catalyst}^{-1}$) from 50 to 450 °C at 2 °C/min and held for 15 hours (total reduction time 18 hours, 2 min). Subsequently, the reactor temperature was reduced to 240 °C, the pressure increased to 13.5 bar, and the catalyst exposed for 250 min to a stream of H_2 and CO in a 2:1 ratio at a space velocity of 383 $mL \cdot min^{-1} \cdot g_{catalyst}^{-1}$.

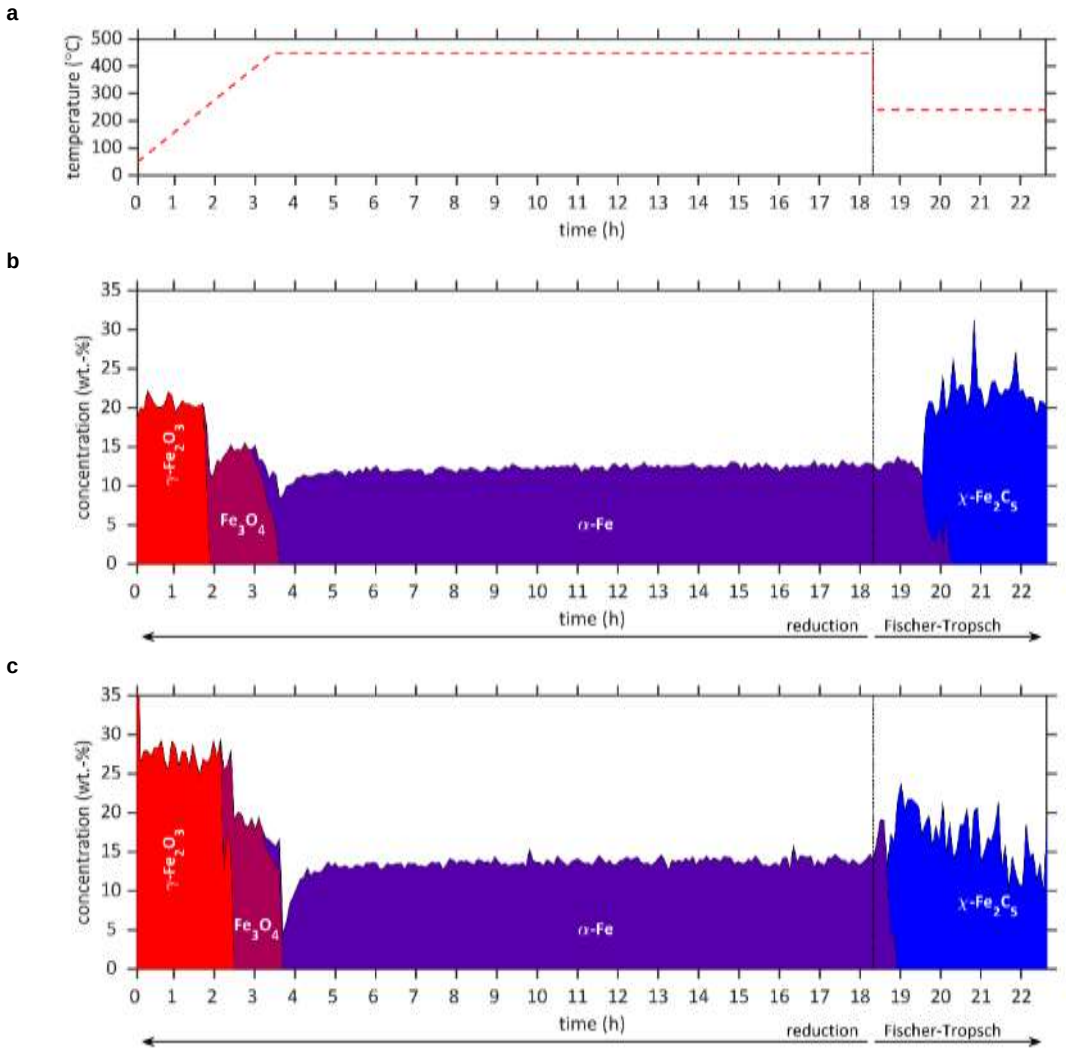

Figure S12. Quantification of *in situ* XRD characterization during reduction and FT synthesis as function of time on stream. **a,** Sample temperature. **b**, Crystalline phase quantification area plot of $Fe/LaAlO_3$ as obtained via Rietveld Refinement. **c**, Crystalline phase quantification area plot of $Fe/La_{0.9}K_{0.1}Al_{0.8}Mn_{0.2}O_3$ as obtained via Rietveld Refinement.

The samples were heated in a continuous flow of H_2 at atmospheric pressure (40 $mL \cdot min^{-1} \cdot g_{catalyst}^{-1}$) from 50 to 450 °C at 2 °C/min and held for 15 hours (total reduction time 18 hours, 2 min). Subsequently, the reactor temperature was reduced to 240 °C, the pressure increased to 13.5 bar, and the catalyst exposed for 250 min to a stream of H_2 and CO in a 2:1 ratio at a space velocity of 383 $mL \cdot min^{-1} \cdot g_{catalyst}^{-1}$.

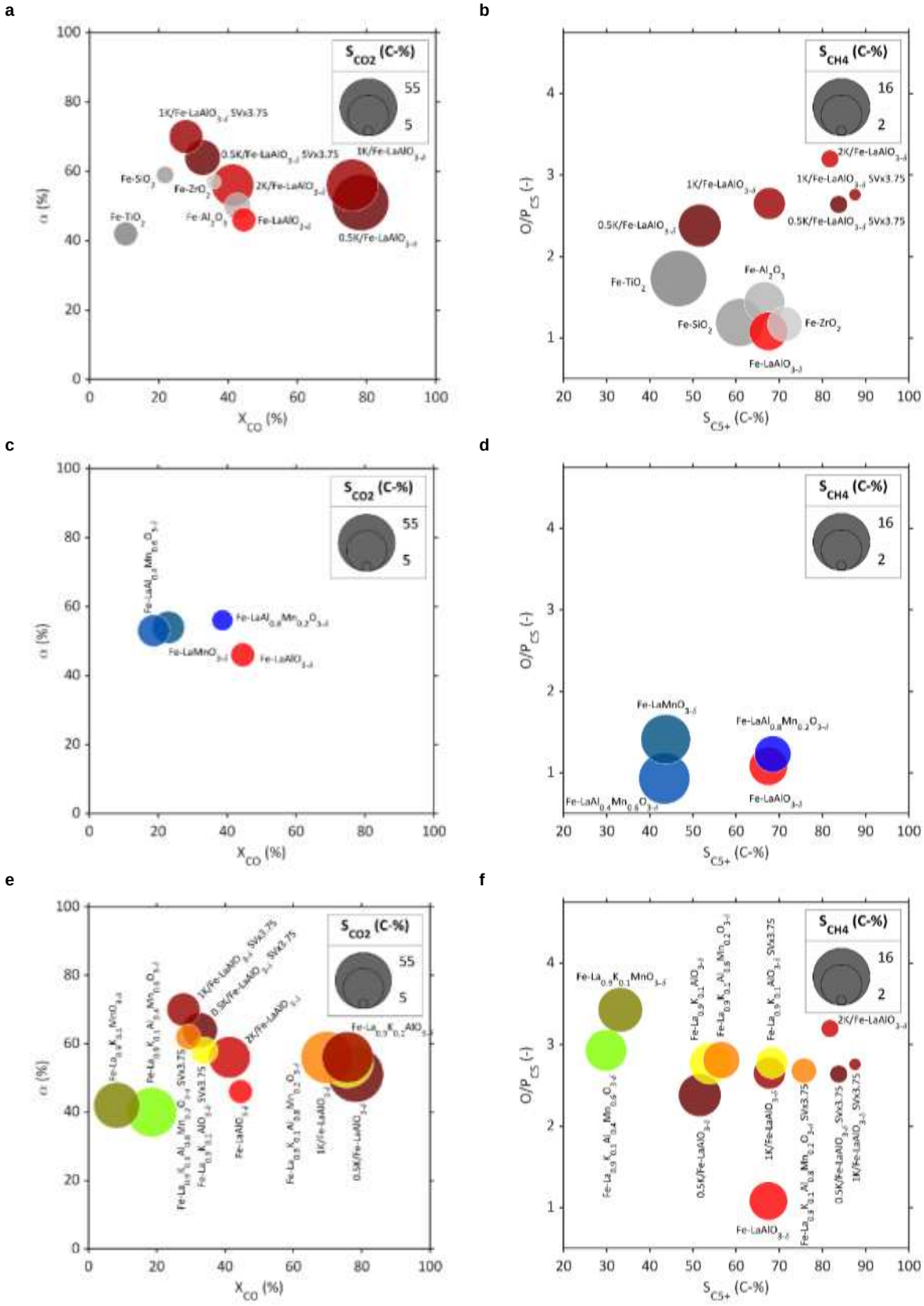

Figure S13. Catalyst performance under Fischer-Tropsch reaction conditions. **a,** Chain growth probability α as a function of CO conversion (X_{CO}) for iron supported on SiO_2, TiO_2, ZrO_2, Al_2O_3, and unmodified $LaAlO_3$, as well as Fe-$LaAlO_{3-\delta}$ promoted with 0.5, 1 and 2 wt.-% potassium. Potassium is introduced before the iron deposition via impregnation. The bubble size represents the CO_2 selectivity (S_{CO2}). **b,** Olefin to paraffin ratio in the C_5 product fraction as a function of the selectivity to hydrocarbons with a carbon number greater than 4 (S_{C5+}) in the

hydrocarbon product of iron supported on SiO_2, TiO_2, ZrO_2, Al_2O_3, and unmodified $LaAlO_{3-\delta}$, as well as Fe-$LaAlO_{3-\delta}$ promoted with 0.5, 1 and 2 wt.-% potassium. Potassium is introduced before the iron deposition via impregnation. The bubble size represents the CH_4 selectivity (S_{CH4}). **c,** Chain growth probability α as a function of CO conversion (X_{CO}) of iron supported on $LaAl_{1-y}Mn_yO_{3-\delta}$ with y = 0, 0.2, 0.6, 1. The bubble size represents the CO_2 selectivity (S_{CO2}). **d,** Olefin to paraffin ratio in the C_5 product fraction as a function of the selectivity to hydrocarbons with a carbon number greater than 4 (S_{C5+}) in the hydrocarbon product of iron supported on $LaAl_{1-y}Mn_yO_{3-\delta}$ with y = 0, 0.2, 0.6, 1. The bubble size represents the CH_4 selectivity (S_{CH4}). **e,** Chain growth probability α as a function of CO conversion (X_{CO}) of iron supported on $La_{1-x}K_xAl_{1-y}Mn_yO_{3-\delta}$ with x = 0, 0.1 and y = 0, 0.2, 0.6, 1. The bubble size represents the CO_2 selectivity (S_{CO2}). For comparison, Fe-$LaAlO_3$ promoted with 0.5, 1 and 2 wt.-% potassium are also displayed. **f,** Olefin to paraffin ratio in the C_5 product fraction as a function of the selectivity to hydrocarbons with a carbon number greater than 4 (S_{C5+}) in the hydrocarbon product of iron supported on $La_{1-x}K_xAl_{1-y}Mn_yO_{3-\delta}$ with x = 0, 0.1 and y = 0, 0.2, 0.6, 1. The bubble size represents the CH_4 selectivity (S_{CH4}). For comparison Fe-$LaAlO_{3-\delta}$ promoted with 0.5, 1 and 2 wt.-% potassium are also displayed.
All FT experiments were carried out in a 600 mL slurry CSTR reactor at 240 °C, 15 bar pressure, a H_2:CO ratio of 2 with 10 vol.-% N_2 as internal standard, and a space velocity of 8 mL·min-1·$g_{catalyst}^{-1}$, except for the samples with the suffix SV × 3.75 where the space velocity was increased to 30 mL·min^{-1}·$g_{catalyst}^{-1}$ to achieve comparable conversion levels. Data collected after 48 h time on stream.

Table S4. CO conversion and selectivity of all evaluated catalysts. All FT experiments were carried out in a 600 mL slurry CSTR reactor at 240 °C, 15 bar pressure, a H_2:CO ratio of 2 with 10 vol.-% N_2 as internal standard, and a space velocity of 8 mL·min-1·$g_{catalyst}^{-1}$, except for the samples with the suffix SV × 3.75 where the space velocity was increased to 30 mL·min^{-1}·$g_{catalyst}^{-1}$ to achieve comparable conversion levels. Data collected after 48 h time on stream.

	X_{CO} (%)	r_{CO}[a] (s^{-1})	α (%)	S_{CO2} (C%)	S_{CH4} (C%)	S_{C2-4} (C%)	S_{C5+} (C%)	S_{CH4} (C%)	S_{C2-4} (C%)	S_{C5+} (C%)	O/P_{C5}[d] (-)
					of total C product[b]			of hydrocarbon product[c]			
Fe-ZrO_2	35.8	5.55E-05	57	7.1	6.5	20.3	66.5	7.0	21.8	71.3	1.2
Fe-Al_2O_3	42.7	6.38E-05	50	14.5	8.0	21.7	59.0	9.0	24.4	66.6	1.4
Fe-SiO_2	21.8	3.42E-05	59	8.4	10.9	25.5	56.4	11.8	27.5	60.8	1.2
Fe-TiO_2	10.4	1.59E-05	42	12.6	13.8	32.9	40.8	15.7	37.6	46.7	1.7
Fe-$LaAlO_{3-\delta}$	44.6	7.35E-05	46	12.7	7.1	21.2	58.8	8.1	24.4	67.5	1.1
2K/Fe-$LaAlO_{3-\delta}$	41.3	6.81E-05	56	31.8	2.0	10.4	55.9	3.0	15.3	81.8	3.2
1K/Fe-$LaAlO_{3-\delta}$	75.9	1.25E-04	56	46.4	3.3	13.9	36.0	6.2	26.2	67.7	2.7
1K/Fe-$LaAlO_{3-\delta}$ SV×3.75	27.8	1.72E-04	70	21.5	1.8	8.0	68.8	2.2	10.2	87.6	2.8
0.5K/Fe-$LaAlO_{3-\delta}$	78.3	1.29E-04	51	54.0	4.5	17.8	23.7	9.7	38.7	51.6	2.4
0.5K/Fe-$LaAlO_{3-\delta}$ SV×3.75	32.7	2.02E-04	64	23.6	2.3	10.1	63.6	3.0	13.3	83.7	2.6
Fe-$LaAl_{0.8}Mn_{0.2}O_{3-\delta}$	38.7	6.37E-05	56	10.6	6.7	21.4	60.9	7.5	24.0	68.5	1.2
Fe-$LaAl_{0.2}Mn_{0.6}O_{3-\delta}$	18.7	2.81E-05	53	19.9	10.6	34.5	34.5	13.3	43.4	43.4	0.9
Fe-$LaMnO_{3-\delta}$	22.9	3.80E-05	54	20.4	10.3	35.7	35.7	12.6	43.7	43.7	1.4
Fe-$La_{0.9}K_{0.1}AlO_{3-\delta}$	75.8	1.16E-04	55	49.7	4.6	18.1	26.7	9.2	36.7	54.0	2.8
Fe-$La_{0.9}K_{0.1}AlO_{3-\delta}$ SV×3.75	34.0	1.89E-04	58	15.6	5.2	21.8	58.2	6.1	25.6	68.3	2.8
Fe-$La_{0.9}K_{0.1}Al_{0.8}Mn_{0.2}O_{3-\delta}$	69.8	1.03E-04	56	47.8	4.0	18.6	29.4	7.7	35.8	56.6	2.8
Fe-$La_{0.9}K_{0.1}Al_{0.8}Mn_{0.2}O_{3-\delta}$ SV×3.75	29.3	1.61E-04	62	14.0	3.8	17.1	65.2	4.4	19.9	75.7	2.7
Fe-$La_{0.9}K_{0.1}Al_{0.4}Mn_{0.6}O_{3-\delta}$	18.6	2.76E-05	70	44.1	5.2	34.0	16.7	9.3	60.9	29.9	2.9
Fe- $La_{0.9}K_{0.1}MnO_{3-\delta}$	8.3	1.18E-05	64	39.2	6.6	35.5	20.9	10.5	56.4	33.2	3.4

[a] Rate of CO conversion (mol_{CO}/mol_{Fe}·s)

[b] Carbon based selectivity including CO_2.

[c] Carbon based selectivity excluding CO_2.

[d] Olefin to paraffin ratio in the C5 hydrocarbon fraction.

Table S5. Elemental composition of perovskite in the spent catalysts. As samples were digested in the presence of an unknown mass of wax, concentrations are normalized to the cationic components of the perovskite structure. Numbers in brackets indicate the targeted composition. Samples used for FT performance at an elevated space velocity of 30 $mL \cdot min^{-1} \cdot g_{catalyst}^{-1}$.

	Composition of perovskite materials			
	La	K	Al	Mn
	(wt.-%)	(wt.-%)	(wt.-%)	(wt.-%)
$La_{0.9}K_{0.1}AlO_{3-\delta}$	81.4 (80.2)	1.9 (2.5)	16.7 (17.3)	0.0 (0.0)
$La_{0.9}K_{0.1}Al_{0.8}Mn_{0.2}O_{3-\delta}$	71.6 (77.4)	1.7 (2.4)	22.6 (13.4)	4.1 (5.2)

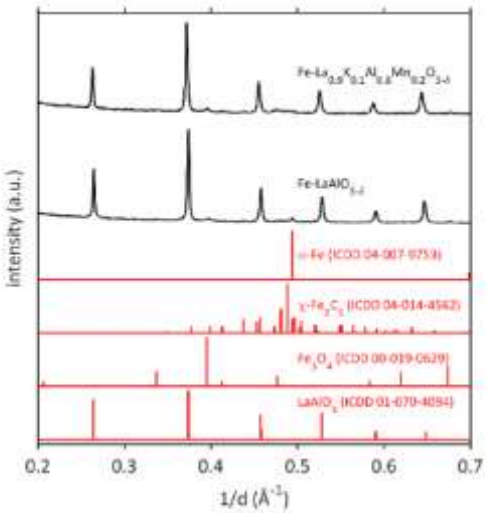

Figure S14. XRD characterisation of spent catalysts. X-ray diffraction patterns of Fe-$LaAlO_{3-\delta}$ and Fe-$La_{0.9}K_{0.1}Al_{0.8}Mn_{0.2}O_{3-\delta}$ after 48 h TOS under FT conditions and extracted from solidified wax via Soxhlet extraction. Reference patterns for $LaAlO_3$ (01-070-1094), Fe_3O_4 (00-019-0629), χ-Fe_2C_5 (04-014-4562) and α-Fe (04-007-9753) from the International Centre for Diffraction Data Powder Diffraction File 4+ 2020.

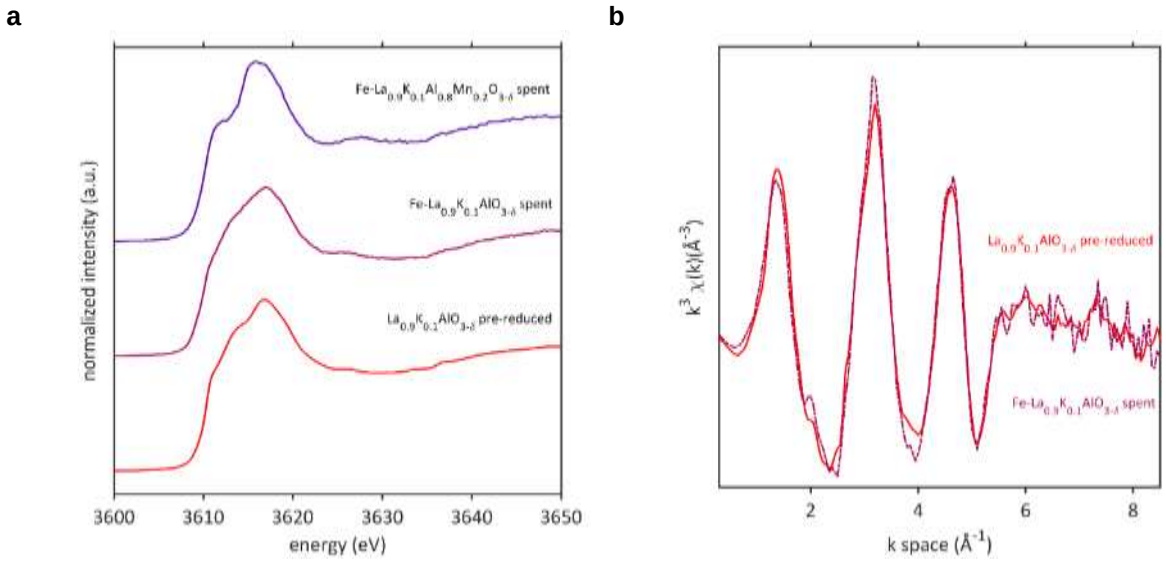

Figure S15. XAS of the potassium K-edge of spent catalysts. **a**, XANES spectra of $La_{0.9}K_{0.1}AlO_{3-\delta}$ pre-reduced, Fe-$La_{0.9}K_{0.1}AlO_{3-\delta}$ spent and Fe-$La_{0.9}K_{0.1}Al_{0.8}Mn_{0.2}O_{3-\delta}$ spent. **b**, EXAFS k^3 weighted spectra of $La_{0.9}K_{0.1}AlO_{3-\delta}$ pre-reduced and Fe-$La_{0.9}K_{0.1}AlO_{3-\delta}$ spent.